UWB-based Indoor Positioning System with Infinite Scalability

Luca Santoro, Matteo Nardello, Davide Brunelli, *Senior Member, IEEE*, Daniele Fontanelli, *Senior Member, IEEE*

***Abstract*—The ultra-wide band radio technology (UWB) is currently considered the de-facto standard for implementing precise indoor positioning systems. Several positioning algorithms are currently being investigated for finding the best implementation in terms of scalability, refresh rate, and energy requirements. Among all the proposed approaches, the Downlink Time Difference of Arrival (DTDoA) is currently considered one of the most promising techniques capable of tracking any number of assets without decreasing the measurement update rate. This paper proposes a model for the DTDoA and validates the algorithms on UWB data, using a motion capture system as ground truth. Results highlight the validity of the previously proposed model, showing that the proposed UWB indoor positioning system achieves a maximum 30 cm uncertainty with only a simple wireless synchronisation, avoiding wired procedure that limits the usability of the infrastructure.**

***Keywords*—Ranging-based positioning, Ultra-Wide Band, Global Positioning System, Positioning, DTDOA, UTDOA, Scalability, Infinite Scalability**

I. Introduction

In the last decades, significant progress was made in the development of positioning systems [1], [2], especially to find a low-cost, accurate and local alternative to GPS for the indoor environment [3]–[6]. This is also thanks to the ground-breaking improvements made to industries such as healthcare [7], [8], livestock farming [9], [10], warehousing [11], [12] and, more recently, in the robotic field [13], [14]. A promising approach to localise a moving entity – with decimetre accuracy level – is assessing Radio Frequency (RF) signal propagation. In the class of RF technology, ultra-wide band (UWB) has attracted increasing interest due to its excellent characteristics, like robustness to multipath error, obstacle penetration, high accuracy, and low cost [15]. In the case of RF-based localisation systems, the fundamentals ranging techniques to estimate the distance from two nodes are: *Received Signal Strength* (RSS); *Time of Arrival* (ToA); *Time Difference of Arrival* (TDoA) and *Angle of Arrival* (AoA). ToA and TDoA ranging techniques are the most commonly used. In ToA, two different communication schemes can be implemented: Single-side (SS) or double-side (DS) two-way ranging (TWR) [16]. With TWR, a synchronisation mechanism between nodes is not required. In fact, accurate calibration of the crystal oscillators is sufficient to achieve the desired accuracy, especially in SS-TWR. The maximum achievable measurements data rate [17] is one of the major drawbacks of TWR, and it depends on the number of messages that the tag has to exchange with the anchors. To overcome this issue, the TDoA approach has been proposed. In this case, a crystal oscillator trimming is not enough to achieve

Authors are with the Department of Industrial Engineering, Via Sommarive 9, 38123, Trento, Italy (e-mail: {luca.santoro, matteo.nardello, davide.brunelli, daniele.fontanelli}@unitn.it)

This article has been accepted for publication in IEEE Transactions on Instrumentation and Measurement. This is the author's version which has not been fully edited and content may change prior to final publication. Citation information: DOI 10.1109/TIM.2023.3282299

the desired accuracy because a tighter synchronisation between the nodes is required. As for the ToA approach, also for TDoA two possible schemes can be implemented. A centralised, or uplink, TDoA (UTDoA) and a decentralised, or downlink, TDoA (DTDoA). Figure 1 presents the DToA and UTDoA approaches. In the first approach, a tag emits a UWB signal, and the difference in the reception times at the anchors side is used to calculate the position of the tag with respect to a reference point [18]. On the contrary, the second transmission scheme mimics a common GPS. The anchors – as the satellites – continuously broadcast timestamped messages that can be received by listening tags/robots. The Uplink Time Difference of Arrival (UTDoA) communication protocol assumes that position information is stored on the infrastructure side, which can be problematic in some applications, e.g., robotic swarm. Sharing position information among all robots can add unnecessary overhead to the estimation process, and installing a router to create a sink node may not always be feasible. The proposed solution is a distributed system where information resides directly on the tag, allowing each entity to choose the right update rate for its calculation without being affected by other tags accessing the information. Notice that the proposed approach generalises the UTDoA, since each entity can in case share the information with the infrastructure, thus resuming the UTDoA paradigm.

In [19], [20] authors developed a DTDoA system, where a tag can determine its position with respect to a reference point exploiting the concurrent ranging (i.e., anchors simultaneously emit a UWB signal). Unfortunately, due to hardware limitations and the precision of the timestamps, the system can achieve a maximum position accuracy in the order of a couple of meters. To mitigate this problem in [21] the authors exploit the idea that each anchor sequentially blinks a message, reducing the error on the estimated position below 1 meter.

According to the literature [22]–[25], the expected

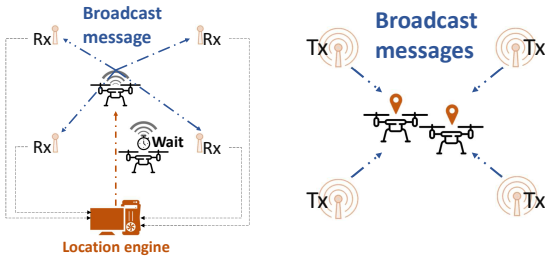

(a) (b)

Fig. 1: In (a) the traditional UTDoA approach where the tag emits the broadcast message, thus limiting the scalability of the system. In (b) the implemented DTDoA approach, where the anchors emit the messages used by the entity to localisation awareness.

positioning accuracy of a UWB system is expected to be at some decimetres. However, the comparison with a ground truth system is quite limited. Mostly due to the the complexity of accurately measuring the *real* real-time position of the tags/robots. To assess the *real* achievable accuracy of a UWB infrastructure for indoor positioning, a ground truth reference can be provided by exploiting a Motion Capture system [26].

This paper uses the innovative DTDoA ranging technique proposed in [25], solving both accuracy and scalability problems of the current state of the art. In particular, scalability is becoming one of the most prominent issues in modern, multi-agent scenarios, such as smart cities [27], Industry 4.0 [28] or more in general scenarios considering a large number of subjects involved [29]. The available solutions with UWB systems suffer of scalability problems in the number of assets simultaneously tracked: in fact, each subject has to complete its localisation phase before other subjects can start their own. Therefore, it becomes fundamental to have a system offering a positioning service with a constant update rate, independent from the number of assets. This paper evaluates and validates the algorithm and highlights how the systems can theoretically scale

to infinity (i.e., any number of assets can be tracked), improving the measurement accuracy with an error in the range of 30 cm, at worst. By temporal-matching the positioning data provided by the UWB infrastructure with the MoCap movement information – used as ground truth – we confirmed the performance of the UWB positioning infrastructure accuracy.

The evaluation is carried out in a structured indoor environment encompassing 8 Qualisys Arqus A9 high-performance cameras[1] providing a position estimation with a much higher accuracy with respect to the UWB infrastructure (down to 0.03 mm). By using the MoCap estimated trajectory as a reference, we validated the UWB one. Results highlights that the effect of the tag motion for the typical human being speed, is negligible. In particular, the main contributions of this paper are:

- We revised the models presented in [25], and we validated the model experimentally with a ground truth provided by optical tracking MOCAP system [26]. Furthermore, we developed a testbed using the sync unit [26] and a wired connection with the UWB receiver.
- We analysed the effect of the tag motion on the positioning and the effect of additional distortions generated by a harsh environment like in our laboratory (small gantry crane, pvc panels).
- We evaluate the performance of the proposed system in both dominant and complete Non-Line-of-Sight (NLoS) conditions, evaluating how the proposed system works in more realistic and complex scenarios.

The rest of the paper is organised as follows. Section II present and discuss the mathematical model of the implemented DTDoA ranging scheme with an analysis of the impact of the uncertainties. In Section III, we present the indoor positioning infrastructure and the relative hardware equipment, together with the experimental validation of the uncertainty models presented. Finally, experimental results and evaluation on the positioning are presented in Section IV. Section V closes this work with final remarks and possible future improvements.

[1]https://cdn-content.qualisys.com/2020/06/PI_Arqus.pdf

II. Measurement models

The Local Positioning System (LPS), detailed in [25], considers an environment with a master UWB, a set of n anchors $\mathbf{a}_i$ and a tag. We can thus denote t as the actual, ideal time and with τ the time measurement from either the master $\tau^m(t)$; the i-th anchor $\mathbf{a}_i$ as $\tau^i(t)$; or the tag $\tau(t)$. Since we do not have an external time reference, we can assume that the time measurements of the master are the reference signal for the UWB positioning algorithm, following the simplified clock model presented in [25], i.e.

$$\tau^{m\star}(t) = o_m + \nu_m t + \eta_m(t) = \tau^m(t) + \eta_m(t), \quad (1)$$

where we use the superscript $\cdot^\star$ to denote each measurement result. o_m is the time offset of the master, $\nu_m = \frac{\overline{f}_m(t)}{f_m}$ the normalised clock rate with respect to the ideal time (i.e., the ratio between the instantaneous frequency of the local oscillator $\overline{f}_m(t)$ and the corresponding nominal value f_m, usually on the order of some part per million (ppm) [30]) and we implicitly assume that the measurement uncertainty $\eta_m(t)$ is a random variable generated by a white, stationary and zero mean process with variance $\sigma^2_{\eta_m}$. Notice that the main source of uncertainties – neglecting the effects of ageing or the drift changes induced by harsh environmental conditions (e.g., mechanical vibrations or temperature effects [30]) – is related to timestamping operations accuracy. Albeit those effects can be mitigated by implementing double consecutive message transmissions, the effect cannot be entirely removed. Similarly, for the i-th anchor $\mathbf{a}_i$ we have

$$\tau^{i\star}(t) = o_i + \nu_i t + \eta_i(t) = \tau^i(t) + \eta_i(t), \quad (2)$$

where o_i and ν_i are the i-th offset and clock rate of the time of the anchors with respect to the ideal time, while $\eta_i(t) \sim \mathcal{N}(0, \sigma^2_{\eta_i})$ and white as before. Finally, for the tag time measurements, we have

$$\tau^\star(t) = o + \nu t + \eta(t) = \tau(t) + \eta(t), \tag{3}$$

where the quantities have the same meaning as in the previous two cases.

A. Anchors clock analysis

The main idea underlying this approach is that no message exchange should be carried out from the tag to the anchors, but only from the anchors to the tag, thus ensuring infinite scalability in terms of trackable number of tags. In the ideal case, the quantities o_i, ν_i (with $i = 1, \ldots, n$) in (2) with respect to the master reference time are retrieved through the following synchronisation algorithm: starting at a generic time $\bar{t}$, the master anchor sends two messages $\tau^m(\bar{t})$ and $\tau^m(\bar{t} + \Delta_{i,m})$ to $\mathbf{a}_i$, whose timestamps at the receiving side are $\tau^i(\bar{t} + \delta_{i,m})$ and $\tau^i(\bar{t} + \Delta_{i,m} + \delta_{i,m})$, where $\delta_{i,m}$ is the Time of Flight (ToF) from the master to the anchor. By denoting with $[x_m, y_m]^T$ and $\mathbf{a}_i = [x_i, y_i]^T$ respectively the master and the anchor known Cartesian coordinates in the $X_w \times Y_w$ plane with respect to a fixed reference frame $\langle W \rangle = \{X_w, Y_w, Z_w\}$, it turns out that

$$\rho_{i,m} = \|[x_m, y_m]^T - \mathbf{a}_i\| = \sqrt{(x_m - x_i)^2 + (y_m - y_i)^2},$$

is the distance among the two anchors. Therefore, assuming that c is the known propagation speed of the radio frequency signal in LOS conditions, we have that the ideal ToF $\delta_{i,m}$ can be obtained as

$$\delta_{i,m} = \frac{\rho_{i,m}}{c}. \tag{4}$$

As a consequence, using (1) and (2) and defining $\overline{\nu}_{i,m} = \frac{\nu_i}{\nu_m}$, we can derive the first-order Taylor approximation for the relative clock rate

$$\overline{\nu}_{i,m}{}^\star = \frac{\tau^{i\star}(\bar{t} + \Delta_{i,m} + \delta_{i,m}) - \tau^{i\star}(\bar{t} + \delta_{i,m})}{\tau^{m\star}(\bar{t} + \Delta_{i,m}) - \tau^{m\star}(\bar{t})} \approx \overline{\nu}_{i,m} + \beta, \tag{5}$$

where the uncertainty mean $\mu_\beta = \mathrm{E}\{\beta\} = 0$ (the $\mathrm{E}\{\cdot\}$ is the usual expected operator), while its variance is

$$\mathrm{E}\{\beta^2\} = \sigma^2_\beta = \frac{2}{\nu^2_m \Delta^2_{i,m}} (\sigma^2_{\eta_i} + \overline{\nu}^2_{i,m} \sigma^2_{\eta_m}).$$

It can thus be argued that the larger the synchronisation interval $\Delta_{i,m}$, the smaller the uncertainty on the indirect measurement of $\overline{\nu}_{i,m}{}^\star$ (i.e., this is the effect of averaging on longer periods).

Similarly, by defining the actual relative offset as

$$\begin{aligned} \overline{o}_{i,m} &= \tau^i(\bar{t} + \delta_{i,m}) - \overline{\nu}_{i,m} \tau^m(\bar{t}) - \delta_{i,m} = \\ &= o_i - \overline{\nu}_{i,m} o_m - (1 - \nu_i)\delta_{i,m}, \end{aligned} \tag{6}$$

we have that

$$\overline{o}_{i,m}{}^\star(\bar{t}) = \tau^{i\star}(\bar{t} + \delta_{i,m}) - \overline{\nu}_{i,m}{}^\star \tau^{m\star}(\bar{t}) - \delta_{i,m} \approx \overline{o}_{i,m} + \gamma(\bar{t}), \tag{7}$$

whose uncertainty has mean $\mu_\gamma(\bar{t}) = \mathrm{E}\{\gamma(\bar{t})\} = 0$ and variance

$$\begin{aligned} \sigma^2_\gamma(\bar{t}) = \mathrm{E}\{\gamma(\bar{t})^2\} = \left(1 - 2\frac{\tau^m(\bar{t})}{\nu_m \Delta_{i,m}}\right) \sigma^2_{\eta_i} + \\ + \overline{\nu}^2_{i,m} \left(1 + 2\frac{\tau^m(\bar{t})}{\nu_m \Delta_{i,m}}\right) \sigma^2_{\eta_m} + \tau^m(\bar{t})^2 \sigma^2_\beta. \end{aligned}$$

Applying (7) to the timestamp quantities delayed by $\Delta_{i,m}$, we have $\overline{o}_{i,m}{}^\star(\bar{t} + \Delta_{i,m})$. It is then possible to formulate a new estimate as

$$\hat{\overline{o}}_{i,m} = \frac{\overline{o}_{i,m}{}^\star(\bar{t}) + \overline{o}_{i,m}{}^\star(\bar{t} + \Delta_{i,m})}{2} = \overline{o}_{i,m} + \overline{\gamma}(\bar{t}), \tag{8}$$

that is now affected by a zero mean uncertainty with variance

$$\sigma^2_{\overline{\gamma}}(\bar{t}) = \frac{\sigma^2_{\eta_i}}{2} + \frac{\sigma^2_{\eta_m}}{2} + \tau^m \left(\bar{t} + \frac{\Delta_{i,m}}{2}\right)^2 \sigma^2_\beta, \tag{9}$$

which may or may not be more useful than (7) depending on the value of $\Delta_{i,m}$. In fact, this is a direct consequence of the correlation between $\overline{o}_{i,m}{}^\star(\bar{t})$ and $\overline{o}_{i,m}{}^\star(\bar{t} + \Delta_{i,m})$ by means of $\overline{\nu}_{i,m}{}^\star$. In this case, the $\Delta_{i,m}$ should be chosen as small as possible. By assuming that the clock rates ν_m and ν_i are approximately constant between two synchronisation periods (usually executed every tens of seconds) and that the master and the anchors do not change their relative positions (i.e.,

the ToF $\delta_{i,m}$ is constant), the relative offset $\overline{o}_{i,m}$ is constant as well. With the previous quantities, we can convert the anchor time scale to the common master time-scale using again a first-order Taylor approximation to have

$$\frac{\tau^{i\star}(t) - \hat{\overline{o}}_{i,m}}{\overline{\nu}_{i,m}{}^{\star}} \approx \tau^m(t) + e_{i,m} + \varepsilon(t). \qquad (10)$$

where $e_{i,m} = \frac{1-\nu_i}{\overline{\nu}_{i,m}}\delta_{i,m}$, $\mathrm{E}\{\varepsilon(t)\} = 0$ and

$$\sigma^2_{\varepsilon}(t) = \frac{\sigma^2_{\eta_i}}{\overline{\nu}^2_{i,m}} + \frac{\sigma^2_{\overline{\gamma}}(\bar{t})}{\overline{\nu}^2_{i,m}} + \\ + \left[\frac{(\tau^m(t) + e_{i,m})^2}{\overline{\nu}^2_{i,m}} - 2\frac{\tau^m(t) + e_{i,m}}{\overline{\nu}^2_{i,m}}\tau^m(\bar{t})\right]\sigma^2_{\beta}.$$

B. Tag clock analysis

Due to the DTDoA approach used, also tag's clock have to be corrected. Let's consider the tag at time t be in position $\mathbf{p}(t) = [x(t), y(t)]^T$ in $\langle W\rangle$. By denoting with

$$\rho_i(t) = \|\mathbf{p}(t) - \mathbf{a}_i\| = \sqrt{(x(t) - x_i)^2 + (y(t) - y_i)^2},$$

the actual distance between the tag and the i-th anchor, we have that the ToF $\delta_i(t)$ is given by (4) when $\rho_{i,m}$ is substituted with $\rho_i(t)$. To perform the algorithm, the relative clock rate $\overline{\nu}_m = \frac{\nu}{\nu_m}$ between the tag and the master (i.e., the reference for all the anchors) is needed and it is computed using the relation (5) specialised for the tag. Therefore, two messages at time t_i and $t_i + \Delta_i$ are received by tag from the i-th anchor and containing the corrected anchor time (10). We first notice that the motion of the tag can induces a variability in the distance to the i-th anchor in the period Δ_i, which is expressed as

$$\rho_i(t_i + \Delta_i) = \|\mathbf{p}(t_i) + d_i(\Delta_i)\mathbf{u}_i(t_i) - \mathbf{a}_i\|,$$

where $d_i(\Delta_i)$ the tag displacement taking place at time t_i in the period Δ_i and $\mathbf{u}_i(t_i)$ it unit direction vector in the plane. An upper bound on the effect of $d_i(\Delta_i)$ can be found noticing that the maximum increase (or decrease) of the distance takes place when $\mathbf{u}_i(t_i) = [x(t) - x_i, y(t) - y_i]^T$, i.e., directed towards the anchor $\mathbf{a}_i$. Therefore the ToF (4) induced variation will be $\delta_i(t_i + \Delta_i) = \delta_i(t_i) + \alpha\frac{d_i(\Delta_i)}{c}$, where $\alpha \in [-1, 1]$ depends on the orientation of $\mathbf{u}_i(t_i)$ as explained before. Therefore, relative clock skew will be affected as well, which will be given by

$$\overline{\nu}_m = \frac{\nu}{\nu_m}\left(1 + \alpha\frac{d_i(\Delta_i)}{c\Delta_i}\right). \qquad (11)$$

For what concerns the TDoA, the two timestamped messages are received by the tag at $\tau^{\star}(t_i + \delta_i(t_i))$ and $\tau^{\star}(t_i + \Delta_i + \delta_i(t_i + \Delta_i))$, both obviously expressed in the tag time-scale. Therefore, using the relation (5), we have

$$\frac{\tau^{\star}(t_i + \Delta_i + \delta_i(t_i + \Delta_i)) - \tau^{\star}(t_i + \delta_i(t_i))}{\frac{\tau^{i\star}(t_i+\Delta_i) - \hat{\overline{o}}_{i,m}}{\overline{\nu}_{i,m}{}^{\star}} - \frac{\tau^{i\star}(t_i) - \hat{\overline{o}}_{i,m}}{\overline{\nu}_{i,m}{}^{\star}}} \approx \\ \approx \overline{\nu}_m + \xi(\Delta_i) = \overline{\nu}_m{}^{\star}, \qquad (12)$$

with $\mathrm{E}\{\xi(\Delta_i)\} = 0$ and

$$\sigma^2_{\xi}(\Delta_i) = \frac{2\overline{\nu}^2_m}{\nu^2_i\Delta^2_i}\sigma^2_{\eta_i} + \frac{2}{\nu^2_m\Delta^2_i}\sigma^2_{\eta} + \frac{\overline{\nu}^2_m}{\nu^2_{i,m}}\sigma^2_{\beta}.$$

C. Indoor GPS TDoA

The UTDoA relies on an implicit event: all the anchors receive a tag's generated broadcast message that acts as an implicit synchronisation event. In the case of the proposed DTDoA with unbounded scalability, the messages are transmitted from anchors side to the tags side, hence a synchronisation event cannot be defined. Strictly speaking, if such a possibility would exist, the master and the anchors would send their packets simultaneously at time t_m. The tag would then measure the difference in reception times as $\tau(t_m + \delta_m(t_m))$ and $\tau(t_m + \delta_i(t_m))$ and, hence be able to compute the TDoA as

$$c\left[\tau(t_m + \delta_i(t_m)) - \tau(t_m + \delta_m(t_m))\right] = \\ = c\nu(\delta_i(t_m) - \delta_m(t_m)) = \nu(\rho_i - \rho_m), \qquad (13)$$

$\forall i = 1, \ldots, n$. Notice that such a measure is only affected by the relative clock rate ν, which is of course negligible since it generates an error in the order of some micrometers.

Since such a synchronised event cannot be generated, at time t_m a broadcast message is transmitted from the master, followed by a second message at time $t_m + \Delta_m$. The tag timestamps the messages at reception times, denoted as $\tau^\star(t_m + \delta_m(t_m))$ and $\tau^\star(t_m + \Delta_m + \delta_m(t_m + \Delta_m))$, and then stores the transmission timestamps $\tau^{m\star}(t_m)$ and $\tau^{m\star}(t_m + \Delta_m)$ encapsulated inside the broadcasted messages. The same mechanism is applied when the anchor i transmits at time t_i and $t_i + \Delta_i$, with tag's transmitted timestamps modified according to (10), which are then used by the tag to compute the relative clock rate (12). The absence of a synchronisation event and the presence of the protocol time interval $\Delta_{i,m} = t_i - t_m$ generates the following protocol-induced uncertainty

$$\begin{aligned} g^\star(\Delta_{i,m}) &= \overline{\nu}_m{}^\star \left(\frac{\tau^{i\star}(t_i) - \hat{\overline{o}}_{i,m}}{\overline{\nu}_{i,m}{}^\star} - \tau^{m\star}(t_m) \right) \approx \\ &\approx \nu \Delta_{i,m} + \nu\alpha \frac{d_i(\Delta_{i,m})}{c} + \overline{\nu}_m e_{i,m} + \varphi(t_i, t_m) \\ &= g(\Delta_{i,m}) + \varphi(t_i, t_m). \end{aligned} \tag{14}$$

In this case $\mathrm{E}\{\varphi(t_i, t_m)\} = 0$ and

$$\begin{aligned} \sigma^2_\varphi(t_i, t_m) &= \overline{\nu}^2_m(\sigma^2_\varepsilon(t_i) + \sigma^2_{\nu_m}) + (\nu_m \Delta_{i,m} + e_{i,m})^2 \sigma^2_\xi(\Delta_i) + \\ &+ \frac{2\overline{\nu}^2_m}{\nu_m \Delta_i}(\nu_m \Delta_{i,m} + e_{i,m})(\sigma^2_\varepsilon(t_i) - \sigma_\varepsilon(t_i, t_i + \Delta_i)), \end{aligned} \tag{15}$$

where $\sigma_\varepsilon(t_i, t_i + \Delta_i)$ is the correlation between the uncertainties $\varepsilon(t_i)$ and $\varepsilon(t_i + \Delta_i)$, given by

$$\begin{aligned} \mathrm{E}\{\varepsilon(t_i)\varepsilon(t_i + \Delta_i)\} &= \frac{(\tau^m(t_i) + e_{i,m})(\tau^m(t_i + \Delta_i)}{\overline{\nu}^2_{i,m}} \sigma^2_\beta + \\ &+ \frac{\sigma^2_{\overline{\gamma}}(\overline{t})}{\overline{\nu}^2_{i,m}} - \frac{\tau^m(t_i) + \tau^m(t_i + \Delta_i) + 2e_{i,m}}{\overline{\nu}^2_{i,m}} \tau^m\left(\overline{t} + \frac{\Delta_{i,m}}{2}\right) \sigma^2_{\overline{\beta}}. \end{aligned}$$

We are now ready to conclude the uncertainty analysis by computing the DTDoA relation (13) with measured quantities

$$\begin{aligned} &c\left[\tau^\star(t_i + \delta_i(t_i)) - \tau^\star(t_m + \delta_m(t_m)) - g^\star(\Delta_{i,m})\right] = \\ &= \nu(\rho_i - \rho_m) - c\overline{\nu}_m e_{i,m} + \lambda(t_i, t_m), \end{aligned} \tag{16}$$

resulting in an overall uncertainty with mean $\mathrm{E}\{\lambda(t_i, t_m)\} = 0$ and variance

$$\sigma^2_\lambda(t_i, t_m) = c^2 \left[2\left(1 + \frac{\nu_m \Delta_{i,m} + e_{i,m}}{\nu_m \Delta_i}\right)\sigma^2_\eta + \sigma^2_\varphi(t_i, t_m) \right]. \tag{17}$$

It is worthwhile to note that those quantities can be equivalently computed for the delayed messages, by considering $\tau^{m\star}(t_m + \Delta_m)$ and $\tau^{\star i}(t_i + \Delta_i)$ in (14), and $\tau^\star(t_m + \Delta_m + \delta_m(t_m + \Delta_m))$ and $\tau^\star(t_i + \Delta_i + \delta_i(t_i + \Delta_i))$ in (16). Of course, comparing (16) and (13), we can notice that the presence of multiple time sources (i.e., having n anchors) induces potential errors stemming from the synchronisation uncertainty with the master $\varepsilon(t)$, highlighted in (10), which is, unfortunately unavoidable.

III. Uncertainty Models Validation

The article [25] showed that the first-order approximation for (17) works remarkably well in simulation. We present here the experimental set-up and the detailed analysis towards experimental validation of the proposed models in an actual environment, also focusing on the detrimental effects of the target motion described in Section II-B, thus deriving the practical relevance of the performed analysis.

A. Indoor testing environment

The testing environment is depicted in Figure 2. The environment is equipped with a MoCap system for ground truth and a network of UWB anchors, described in what follows. It has to be noted that the laboratory in which the system has been tested is very challenging (see Figure 3), due to the presence of many artefacts generating additional sources of uncertainty on the LPS.

1) MoCap system: To create a ground truth trajectory to evaluate the accuracy of the UWB positioning system, we have adopted a Motion Capture system, specifically a system provided by Qualisys with 8 Arqus A9 cameras, a sync unit, and the workstation for system

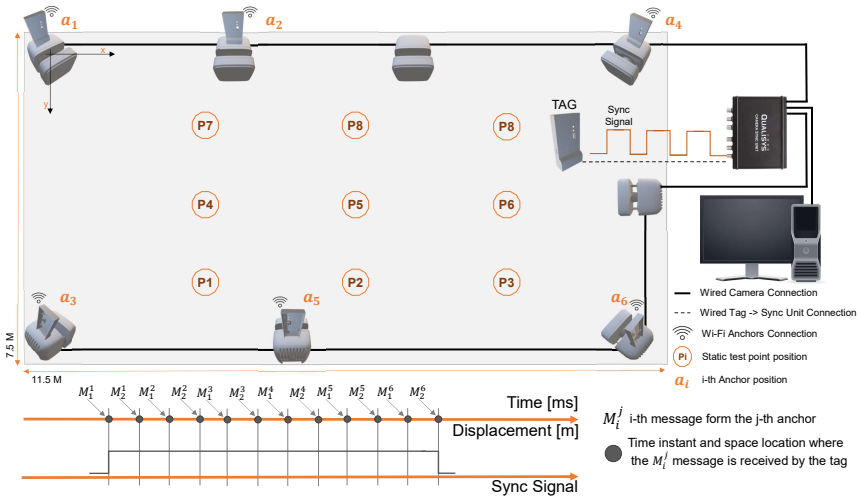

Fig. 2: Indoor testing infrastructure. In the top, we show the MoCap cameras along with the UWB anchors and the acquisition chain. The bottom part depicts the effect of tag moving affecting reception's time instant and the spatial location of the 12 messages sent by the $n = 5$ reference anchors (the sixth is the master). Each message is received at a different time/space instant/location, causing the estimation shifting problem. The highlighted P_i locations show where the static tests were conducted.

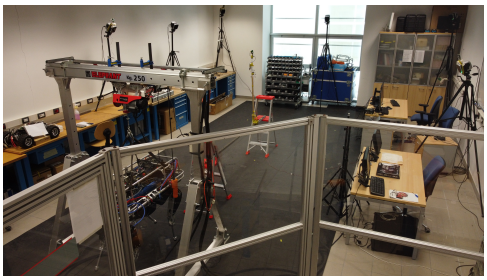

Fig. 3: Laboratory environment. In particular, the quadruped and barrier for the anthropomorphic robotic arm created the conditions for the multi-path effect and NLoS condition, respectively.

configuration (see Figure 2). The cameras are configured to work at a frequency of 240 Hz to achieve a suitable frame rate with respect to the UWB data rate. The tag is equipped with a Hand Rigid Bodies Marker and tracked by the MoCap software, measuring its 3D position at each captured frame. After calibration, the system reports a sub-millimetre accuracy with less than 1 mm standard uncertainty [2].

2) UWB system: To implement our LPS, we decided to use the commercial-off-the-shelf COTS) Decawave DWM1001[3] SoM, a customary choice for indoor positioning systems [31]. The DWM1001 is a compact module that integrates both a low-power nRF52832 MCU and the Decawave DW1000[4] UWB transceiver. It also integrates RF circuitry, a UWB antenna, and a motion sensor for sensor fusion applications [32].

The DW1000 chip is an IEEE 802.15.4-2011 [33] compliant UWB transceiver, which can operate on six different frequency bands with centre frequencies

[2]The adopted calibration procedure can be found here https://docs.qualisys.com/getting-started/content/getting_started/running_your_qualisys_system/calibrating_your_system/ calibrating_your_system.html

[3]https://www.decawave.com/sites/default/files/dwm1001_datasheet.pdf

[4]https://www.decawave.com/sites/default/files/resources/dw1000-datasheet-v2.09.pdf

between 3.5 to 6.5 GHz and bandwidth of 500 or 900 MHz. It provides the possibility of ranging measurements and retrieving the measured CIR. The chip also offers three different data rates: 110 kbps, 850 kbps, and 6.8 Mbps. The DW1000 clocking scheme is based on three main circuits; crystal oscillator (trimmed in production to reduce the initial frequency error to approximately 3 ppm), Clock Phase-Locked Loop (PLL), and RF PLL. The on-chip oscillator is designed to operate at a frequency of 38.4 MHz. This clock is then used as the reference input to the two on-chip PLLs. The clock PLL generates a 63.8976 GHz reference clock required by the digital backend for signal processing. The RF PLL generates the clock for the receive and transmit chain. The DW1000 automatically timestamps transmitted and received frames with a precision of 40 bits. Working at a nominal 64 GHz resolution, packets are timestamped with a 15.65 ps event timing precision[5].

The DWM1001 SoM was configured, during the experimental tests, to use UWB Channel 5 (with a frequency of 6489.6 MHz and a bandwidth of 499.2 MHz) preamble length of 128 symbols, the highest Pulse Rate of 64 MHz and the highest Data Rate of 6.8 Mbps.

To implement the LPS method on UWB, a specific number of DWM1001 modules are programmed to act as anchors to provide a reference infrastructure for the tags. Hence, each anchor is interfaced with a Raspberry PI 3 and a DWM1001 module. Finally, data sharing and acquisition is implemented by leveraging the MQTT protocol to enable data transfer by a remote system. To create an infrastructure referenced by the motion capture, we have installed the UWB anchors on top of the MoCap cameras, while the MoCap sync unit is connected with a wired cable to one of the GPIO of the DWM1001's MCU of the tag for synchronisation of all the sensor readings. Indeed, the sync unit allows external recording events and matching them with the captured frames. Given the standard uncertainty of the MoCap system previously mentioned and the typical accuracy of the UWB positioning system (typically, in the order of some centimetres), we limit the uncertainty analysis to 1 mm of minimum resolution.

The infrastructure parameters for the algorithm are: $\Delta_{i,m} = 3$ ms, $\Delta_i = 1.1$ ms, $\rho_{i,m} = \{6.063, 11.230, 9.716, 7.484, 4.048\}$ m for the $n = 5$ anchors, $c = 299792458$ m/s.

B. Model validation

Notice that, to validate the final DTDoA uncertainty (17), the compounding experimental quantities must be retrieved, which are impossible to be gathered from any measurement system. Therefore, we adopt a mixture of simplifications and nominal values to validate the equation.

The results presented in this section refer to the static case, i.e., where $\alpha = 0$ in (11) and (14). We first analyse the synchronisation period $\Delta_{i,m}$ influence, as mentioned in Section II-A. Indeed, there is a linear dependency between the offset estimation error $\tilde{o}_{i,m} = \hat{o}_{i,m} - o_{i,m}$ and $\Delta_{i,m}$, which is empirically evaluated to be $\tilde{o}_{i,m} \approx 8 \cdot 10^{-6} \Delta_{i,m}$ (e.g., for $\Delta_{i,m} = 10$ ms, $\tilde{o}_{i,m} = 80$ ns). Similarly, increasing the anchors transmission delay $\Delta_{i+1,m} - \Delta_{i,m}$ of some milliseconds, the relative clock rate estimation error $\hat{\nu}_{i,m} - \nu_{i,m}$ increases of some ppm. We then recall that the reference time for our platform is given by the master clock, hence we assume for the model (1) that $\nu_m = 1$, so as that (14) turns to

$$g^\star(\Delta_{i,m}) = (\nu + \xi(\Delta_i)) \left(\frac{\tau^{i\star}(t_i) - \hat{\tilde{o}}_{i,m}}{(\nu_i + \beta)} - \tau^{m\star}(t_m) \right) \approx$$

$$\approx \nu(\Delta_{i,m} + e_{i,m}) + \varphi(t_i, t_m).$$

Moreover, considering the standard uncertainty of the DWM1001's clock of 10 ppm [34], we assume that $\sigma_{\eta_m} = \sigma_{\eta_i} = \sigma_\eta = 0.45$ ns for all the uncertainty sources in (1), (2) and (3). Given these rated uncertainties and the fact that the involved time intervals $\Delta_{i,m}$

[5]https://www.decawave.com/dw1000/usermanual/

TABLE I: Experimental standard uncertainty $\overline{\sigma}_\lambda(t_i, t_m)$ collected from the positions reported in Figure 2. All the quantities are expressed in millimetres and should be compared with the model-based value of the standard uncertainty $\sigma_\lambda(t_i, t_m)$. Results are the same for all the testing positions P_1, P_2, ..., P_9 in Figure 2.

Anchors	1	2	3	4	5
$\overline{\sigma}_\lambda(t_i, t_m)$	97	125	147	167	184
$\sigma_\lambda(t_i, t_m)$	72	93	110	124	137

and Δ_i are in the order of few milliseconds, we can safely assume for the sake of validation that $\nu \approx 1$, thus (17) turns to

$$\sigma^2_\lambda(t_i, t_m) = c^2 \left[2 \left(1 + \frac{\frac{\tau^{i\star}(t_i) - \hat{\overline{o}}_{i,m}}{\nu_i} - \tau^{m\star}(t_m)}{\Delta_i} \right) \sigma^2_\eta + \sigma^2_\varphi(t_i, t_m) \right]. \quad (18)$$

The only missing ingredient is $\sigma^2_\varphi(t_i, t_m)$ in (15), which is experimentally retrieved by directly computing the variance of (14), i.e., of the measured quantities $\frac{\tau^{i\star}(t_i) - \hat{\overline{o}}_{i,m}}{\overline{\nu}_{i,m^\star}} - \tau^{m\star}(t_m)$. Hence, with the described approach, we had the theoretical standard uncertainty $\sigma_\lambda(t_i, t_m)$ reported in Table I. This value is then compared with the experimental standard uncertainty $\overline{\sigma}_\lambda(t_i, t_m)$ retrieved from the MoCap described in Section III-A and considering 5000 UWB samples from each position (see Table I). In both cases, the standard uncertainties are independent from the testing positions $P_1, \ldots, P_9$ depicted in Figure 2, while the terms governing the equations are $\Delta_{i,m}$, σ^2_η and $\sigma^2_\varphi(t_i, t_m)$. Notice that the theoretical overall DTDoA uncertainty model (17) approaches remarkably well the results obtained in the field. Moreover, the synchronisation algorithm among the infrastructure nodes makes the proposed solution rather flexible and allows new receivers to join the network without any particular calibration procedure or reset of the infrastructure, which partially induces a part of the uncertainties subsumed in the statistical analysis of Table I.

TABLE II: Comparison between the theoretical nonlinear value (18) and the CRLB. All the quantities are expressed in mm^2.

Anchor	1	2	3	4	5
Nonlinear (18)	3	10	21	37	55
CRLB	1	3	7	12	18

To further substantiate the analysis, we first experimentally verified that the DTDoA measurements actually follow a biased Gaussian distribution, with a bias that is mainly induced by non line of sight conditions and delays in the message timestamp processing times. Then we carried out a Cramer-Rao Lower Bound (CRLB) analysis as reported in [35] to be compared to the nonlinear (i.e., without first-order approximations) version of (18), both reported in Table II. As can be seen, the analysis carried out is a good approximation of the actual CRLB, thus further validating the proposed analysis. Notice that the uncertainty is a function of the anchor position, thus showing a perfect match with the importance of anchor deployment geometry [36]. Moreover, as mentioned in Section II-A, $\Delta_{i,m}$ should be chosen as small as possible to limit the uncertainty: from Table II, it is evident a quadratic dependency for both the CRLB and the nonlinear (18) (indeed, $\Delta_{i,m} < \Delta_{i+1,m}$ as aforementioned), which, instead, is lost for the first order linearised values in Table I. Nevertheless, by comparing the standard deviations in Table I and the variances in Table II, it turns out that (17) is a good approximation of the nonlinear version of (18) despite the first-order approximations adopted, and thus can be considered as a nice figure of merit for the proposed solution.

C. Effect of a moving tag

We now investigate the effects of the tag motion, thus $\alpha \neq 0$ and unknown in (11) and (14). The main effect is dictated, once again, by the absence of a synchronisation event for the infrastructure, hence when the tag starts to move, the anchor timestamped values are acquired at different locations as shown at the bottom of Figure 2: the position signed as M_i^j stand for the i-th message ($i = 1, 2$) form the j-th anchor ($j = 2, \ldots, 5$, being $j = 1$ the master). Therefore, it is not defined as a unique position from the MoCap to act as the ground truth. Therefore, we decided to compare the DTDoA estimated values with three sample points: with reference to Figure 2, the first position M_1^1, the average position $\overline{M} = \frac{1}{2(n+1)} \sum_{j=1}^{5} M_1^j + M_2^j$ and the last position M_2^6. To synchronise the tag and the MoCap, we used the wired connection described in Section III-A and, in particular, we raised the GPIO of the DWM1001's MCU at M_1^1 and lowered at M_2^6, thus defining the UWB positioning cycle. It is worth to be noted that since $\Delta_i = 1.1$ ms and the sync unit maximum event capture rate is equal to 200 Hz, it was not possible to capture all the intermediate positions in the middle of the positioning cycle. To circumvent this limitation, the experimental setup comprised two support to hold a prismatic guide on which a vertical bar is mounted on the carriage. The experiment is performed over a distance of 3 m and moving the carriage linearly at a constant speed of about 1 m/s (e.g., an average walking speed of a human being) and only the first M_1^1 and last M_2^6 position of each positioning cycle were actually stored (see the bottom of Figure 2): with this setup, the average positions were computed correctly as well.

Nevertheless, such drawback makes the analysis of $\sigma_\lambda^2(t_i, t_m)$ in (17) carried out previously hard to be pursued. Therefore, we decided to consider the effect of the motion of the tag on the standard uncertainty of the estimated position. To this end, we adopted the standard Least Squares (LS) solution that can be found in [37]. Hence, the mean error on the X_w and Y_w axes computed on 5000 position cycles are reported in Table III. It is evident how the tag's motion induces a constant bias, which is a consequence of the linear motion of the tag generating the effect described in Section II-B, no matter the adopted ground truth reference and that the UWB positioning system underestimates the tag position. We also report in Figure 4 the probability mass function of the positioning error for the moving tag. Since the standard uncertainties, in this case, are $\sigma_x = 67$ mm and $\sigma_y = 78$ mm along the X_w and Y_w reference axes, they are comparable to standard deviations of the positioning experiments in Section IV, hence implying that the effect of the tag motion, for the typical human being velocity, is negligible in (17). It has to be noted that the proposed indoor positioning system is conceived for pedestrians or objects moving inside indoor environments. While such environments make the restriction to 2D scenarios quite natural, they also impose potential constraints once 3D problems are considered, since the anchor deployment is typically restricted by the presence of furniture or production machinery. As such, the anchors are most often placed at similar heights, thus increasing the uncertainty on the third dimension (i.e., Vertical Dilution of Precision (VDoP) issue [38]). In robotic systems, like Unmanned Aerial Vehicles (UAVs), where the z-coordinate plays a

TABLE III: Mean error of the UWB position estimates on 5000 position cycles for a linearly moving tag with respect to the three ground truth references. All the quantities are reported in millimetres.

	M_1^1	$\overline{M}$	M_2^6
μ_x	-93	-93	-94
μ_y	-173	-174	-173

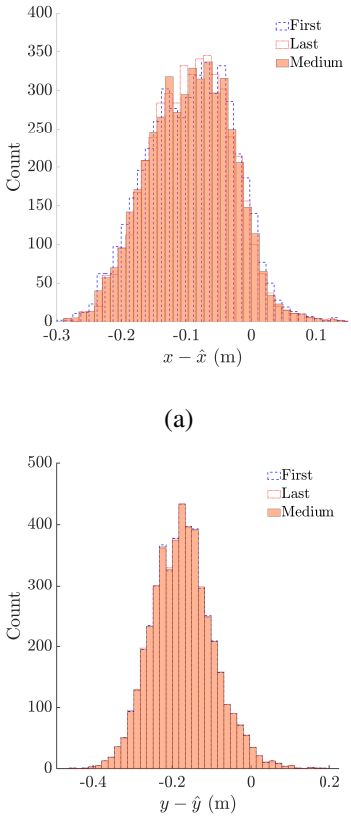

Fig. 4: Histogram of the error for the dynamic test along the X_w (a) and Y_w (b) reference axes over 5000 repeated measurements.

crucial role in navigation, obtaining accurate altitude information is paramount. To this end, additional sensors such as barometers, ultrasonic sensors, Time-of-Flight (ToF) sensors, and LIDAR can be integrated into the system. The data from these sensors can then be fused to produce a more precise position estimation. An ad-hoc anchor deployment to account for this additional issue for 3D problems is a challenging research problem per se, thus left for future investigations.

IV. Positioning Results

We now present the results on the position of the tag that can be attained by the proposed solution by applying the mentioned multilateration solution for the

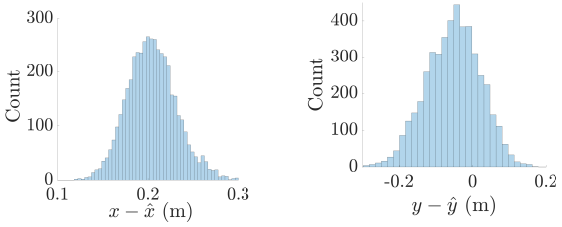

Fig. 5: Distribution of the error in the static positions of Figure 2 along the X_w (a) and Y_w (b) over 5000 repeated measurements.

TDoA. As a first comment, the validation analysis in Section III shows clearly that the standard LS solution can be adopted to solve the multilateration problem of the DTDoA, being a Weighted LS useless (i.e., the $\sigma^2_\lambda(t_i, t_m)$ in (17) is the same for all the anchors).

To evaluate the accuracy of the proposed system, we collected 5000 samples of a static tag in the positions P_i reported in Figure 2 and with the same choice of the parameters reported in Section III. Figure 5 shows the empirical probability mass function of the positioning error with respect to the ground truth of the MoCap system. Despite the closeness to a Gaussian-shaped curve obtained (which has been correctly assumed throughout the analysis of Section III), the distribution presents a bias induced by the previously mentioned angle-dependent UWB pulse distortion and path overlaps [39]. Moreover, the measure is also subjected to the anchors deployment geometry in the testing room that may cause reflections due to the presence of metallic objects (see Figure 3). In particular, the bias is quantifiable in $\mu_x = 203$ mm and $\mu_y = -49$ mm for the X_w and Y_w axes, respectively, while the standard uncertainty is $\sigma_x = 27$ mm and $\sigma_y = 69$ mm. To summarise, also considering the dynamic conditions reported in Figure 4, we can claim a positioning error that is below 30 cm, specifically a 2σ of 156 mm, and with an

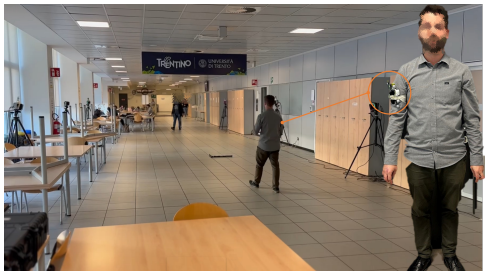

Fig. 6: Experimental setup inside the hall of the "Dipartimento Ingegneria Industriale" of the University of Trento. Inside the orange circle the receiver mounting point on the tester arm.

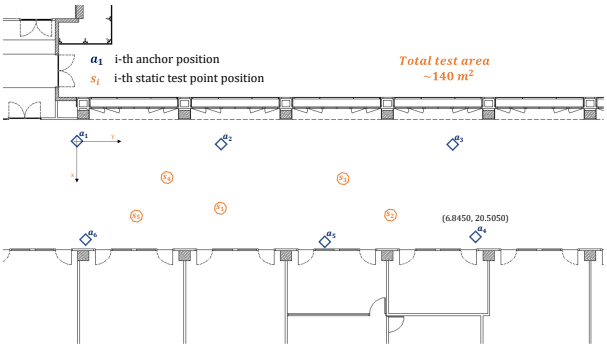

Fig. 7: Graphical representation of the experimental setup, with the static testing point reported.

arbitrary number of positioned tags. To further assess the proposed system, we test the proposed solution in a larger area, as shown in Figure 6. Both static and dynamic tests are reported to assess the performance of the system in a natural scenario. In Figure 7, both the positions of the UWB anchors and the static tested points are reported, while Table IV shows the mean error and the standard deviation in those static locations. In the same area, the dynamic tests are instead organised adopting two challenging paths: 8-shaped and Z-shape patterns, whose actual and estimated trajectories are reported in Figure 8. The result of the dynamic tests are reported in Table V. The results of these experimental tests confirm how the environment affects performance:

TABLE IV: Mean error $\{\mu_x, \mu_y\}$ and standard deviation $\{\sigma_x, \sigma_y\}$ along the X and Y axis, respectively, and computed in the five locations of Figure 7. All the quantities are expressed in millimetres.

Test Point	μ_x	μ_y	σ_x	σ_y
s_1	7	-56	119	82
s_2	50	-91	141	128
s_3	98	-92	166	111
s_4	131	-84	174	115
s_5	170	59	242	196

the mean error is indeed smaller than the one observed in Figure 4 due to the favourable environmental conditions for the initial wireless synchronisation and despite the more challenging trajectories adopted (in Figure 8-(b) it is possible to appreciate the antenna pattern effect at the sharp turns). The standard deviation, instead, is considerably increased due to the arm-mounted receiver position (See Figure 6), generating several NLoS conditions. We finally analyse the effect on the choice of the positioning cycle length. Indeed, at a first glance, making Δ_i large may have a positive effect on $\sigma^2_\lambda(t_i, t_m)$ in (17) (and, hence, on the positioning accuracy). However, $\Delta_{i,m}$ enters several times in the computation of the final uncertainties: for instance,

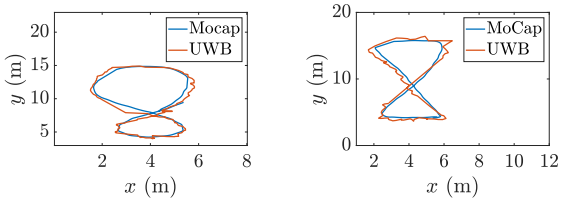

(a) (b)

Fig. 8: Dynamic test trajectories: 8-shape pattern (a) and Z-shape pattern (b). The trajectories are executed by the tester in the area depicted in Figure 6.

TABLE V: Mean error $\{\mu_x, \mu_y\}$ and standard deviation $\{\sigma_x, \sigma_y\}$ for the dynamic tests of Figure 8. All the quantities are expressed in millimetres.

Pattern	μ_x	μ_y	σ_x	σ_y
Z-shape	45	8	207	201
8-shape	29	36	238	245

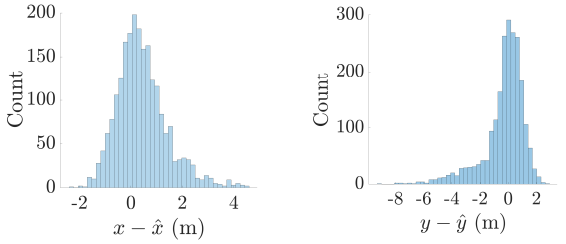

(a) (b)

Fig. 9: Distribution of the error in the static positions of Figure 2 along the X_w (a) and Y_w (b) over 5000 repeated measurements and with $\Delta_{i,m} = 16$ ms.

the large is Δ_i, the more will be the synchronisation uncertainty due to the incorrect clock tag drift ν (3). We propose here empirical proof using the resulting positioning uncertainties as a figure of merit. Let us recall that $\Delta_{i,m} = 3$ ms, hence having $n = 5$ anchors (the first is the master), this corresponds to a positioning cycle of 15 ms. By setting $\Delta_{i,m} = 16$ ms, we obtain the empirical probability mass function in Figure 9 for the positioning error over 5000 repetitions. It can be immediately noticed how the effect of the not modelled nuisances becomes remarkable, generating quite long tails in the distribution. Moreover, we have $\mu_x = 288$ mm (with $\sigma_x = 797$ mm) and $\mu_y = -323$ mm (with $\sigma_y = 1.01$ m), i.e., highly noticeable detrimental effects. This is also reflected in the experimental value of (17), which turns to $\sigma_\lambda(t_i, t_m) = 279$ mm. Therefore, the longer is $\Delta_{i,m}$, the worse is the positioning accuracy,

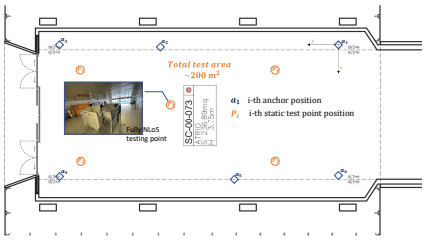

Fig. 10: Graphical representation of the experimental setup, with the static testing point reported.

which verifies the hypothesis in [40].

A. *Validation in challenging scenarios*

To further experimentally validate the proposed positioning system, we report here tests under different scenarios, including those with dominant NLoS conditions as well as under completely NLoS conditions. The experimental setup arena is the hall of our department shown in Figure 10. The area comprises obstacles and vending machines, while the experiments have being conducted in a working day populated with many students. The system was firstly tested at static points $[P_1, P_2, P_3, P_4, P_5]$ selected to cover an area from the infrastructure boundary, where the positioning performance is known to be reduced due to the Position Dilution of Precision (PDoP) [38] value, to the center of the area. Metal bulletin boards were intentionally placed in the middle to introduce dominant NLoS conditions during the tests at points $[P_1, P_2, P_3, P_4]$, obstructing the propagation of the UWB signal with at least three anchors. The experiment resulted in a maximum of 30 cm of uncertainty, consistent with the previously reported results. The point $P5$ was tested under fully NLoS conditions by creating a barrier using the metal bulletin boards, resulting in worse performance compared to the results obtained for the testing point s_1 of Figure 10 that present a similar spatially relationship with the anchors. The results of this experiment are

TABLE VI: Mean error $\{\mu_x, \mu_y\}$ and standard deviation $\{\sigma_x, \sigma_y\}$ along the X and Y axis, respectively, and computed in P_5 of Figure 10. All the quantities are expressed in millimetres.

Test Point	μ_x	μ_y	σ_x	σ_y
P_5	210	-270	125	245

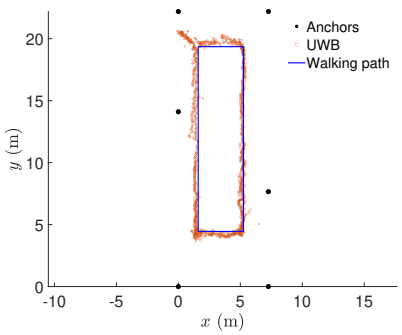

Fig. 11: Dynamic test trajectory. The tester walks along a predefined path.

reported in Table VI. We additionally consider dynamic tests in the same scenario. Unfortunately, since NLoS conditions are present, the motion capture system was not available (indeed, it works only when Line-of-Sight conditions hold). Therefore, we used fiducial points to walk through. The results obtained from this approach, albeit qualitative due to the explained shortcomings, are shown in Figure 11, demonstrating once more the effectiveness of the proposed solution in dynamic and natural populated environments.

V. Conclusion

This paper presents the solution to the scalability problem of LPSs. The introduced DTDoA scheme enables the possibility to supply the pose information to an infinite number of entities (e.g., human beings, robots) endowed with a UWB receiver. The analysis of the uncertainties (both theoretical and experimental) highlighted the critical points for the DTDoA scheme, and it guided the development of an LPS with a maximum position error below 30 cm in challenging scenarios. The maximum pose information update rate reached in this work is 67 Hz. In future work, we investigate alternative downlink schemes to increase the update rate of the positioning information, removing the limit given by the number of active anchors and, thus, reducing the positioning cycle $n\Delta_i$. To derive theoretical results that can be compared with experiments, a simplified clock model that explicitly neglects the non-perfect-isotropic radiation pattern effect and the delay introduced by the internal circuitry (which are, however, implicitly analysed through experimental evidence) is considered. The theoretical and experimental results obtained from this work lay the foundation for the development of state estimators and navigation solutions onboard to reduce the receiver velocity measurement uncertainty. The next step is to collect an adequate dataset from an autonomous robot exploiting this solution and introducing the neglected effects of this first model, improving the trueness of the raw measurements, enabling the possibility to investigate the development of data fusion techniques, compensating NLOS and multipath effects and further validating the proposed system.

Acknowledgments

This research received funds by Fondazione VRT - Fondazione per la Valorizzazione della Ricerca Trentina.

References

[1] N. Saeed, H. Nam, T. Y. Al-Naffouri, and M.-S. Alouini, "A state-of-the-art survey on multidimensional scaling-based localization techniques," *IEEE Commun. Surveys Tuts.*, vol. 21, no. 4, pp. 3565–3583, 2019.

[2] J. Karl, *Celestial navigation in the GPS age*. Paradise Cay Publications, 2007.

[3] G. Seco-Granados, J. López-Salcedo, D. Jiménez-Baños, and G. López-Risueño, "Challenges in indoor global navigation satellite systems: Unveiling its core features in signal processing," *IEEE Signal Processing Magazine*, vol. 29, no. 2, pp. 108–131, 2012.

[4] M. Maheepala, A. Z. Kouzani, and M. A. Joordens, "Light-based indoor positioning systems: A review," *IEEE Sensors Journal*, vol. 20, no. 8, pp. 3971–3995, 2020.

[5] T. Kim Geok, K. Zar Aung, M. Sandar Aung *et al.*, "Review of indoor positioning: Radio wave technology," *Applied Sciences*, vol. 11, no. 1, 2021.

[6] P. Pascacio, S. Casteleyn, J. Torres-Sospedra *et al.*, "Collaborative indoor positioning systems: A systematic review," *Sensors*, vol. 21, no. 3, 2021.

[7] Y. Yin, Y. Zeng, X. Chen, and Y. Fan, "The internet of things in healthcare: An overview," *Journal of Industrial Information Integration*, vol. 1, pp. 3–13, 2016.

[8] S. de Miguel-Bilbao, J. Roldán, J. García *et al.*, "Comparative analysis of indoor location technologies for monitoring of elderly," in *2013 IEEE 15th International Conference on e-Health Networking, Applications and Services (Healthcom 2013)*, 2013, pp. 320–323.

[9] K. Ren, J. Karlsson, M. Liuska *et al.*, "A sensor-fusion-system for tracking sheep location and behaviour," *International Journal of Distributed Sensor Networks*, vol. 16, no. 5, 2020.

[10] S. Koompairojn, C. Puitrakul, T. Bangkok *et al.*, "Smart tag tracking for livestock farming," in *2017 10th International Conference on Ubi-media Computing and Workshops (Ubi-Media)*, 2017, pp. 1–4.

[11] E. Sun and R. Ma, "The uwb based forklift trucks indoor positioning and safety management system," in *2017 IEEE 2nd Advanced Information Technology, Electronic and Automation Control Conference (IAEAC)*, 2017, pp. 86–90.

[12] B. Ivsic, J. Bartolic, Z. Sipus, and J. Babic, "Uwb propagation characteristics of human-to-robot communication in automated collaborative warehouse," in *2020 IEEE International Symposium on Antennas and Propagation and North American Radio Science Meeting*, 2020, pp. 1125–1126.

[13] H. Obeidat, W. Shuaieb, O. Obeidat, and R. Abd-Alhameed, "A review of indoor localization techniques and wireless technologies," *Wireless Personal Communications*, vol. 119, no. 1, pp. 289–327, Jul 2021. [Online]. Available: https://doi.org/10.1007/s11277-021-08209-5

[14] M. S. Mozamir, R. B. A. Bakar, and W. I. S. W. Din, "Indoor localization estimation techniques in wireless sensor network: A review," in *2018 IEEE International Conference on Automatic Control and Intelligent Systems (I2CACIS)*, 2018, pp. 148–154.

[15] A. Alarifi, A. Al-Salman, M. Alsaleh *et al.*, "Ultra wideband indoor positioning technologies: Analysis and recent advances," *Sensors*, vol. 16, no. 5, 2016. [Online]. Available: https://www.mdpi.com/1424-8220/16/5/707

[16] C. L. Sang, M. Adams, T. Hörmann *et al.*, "An analytical study of time of flight error estimation in two-way ranging methods," in *2018 International Conference on Indoor Positioning and Indoor Navigation (IPIN)*, 2018, pp. 1–8.

[17] V. Magnago, P. Corbalán, G. Picco *et al.*, "Robot Localization via Odometry-assisted Ultra-wideband Ranging with Stochastic Guarantees," in *Proc. IEEE/RSJ International Conference on Intelligent Robots and System (IROS)*. Macao, China: IEEE, Nov. 2019, pp. 1607–1613.

[18] Y. Cheng and T. Zhou, "Uwb indoor positioning algorithm based on tdoa technology," in *2019 10th International Conference on Information Technology in Medicine and Education (ITME)*, 2019, pp. 777–782.

[19] P. Corbalán, G. P. Picco, and S. Palipana, "Chorus: Uwb concurrent transmissions for gps-like passive localization of countless targets," in *2019 18th ACM/IEEE International Conference on Information Processing in Sensor Networks (IPSN)*, 2019, pp. 133–144.

[20] R. Zandian and U. Witkowski, "Robot self-localization in ultra-wideband large scale multi-node setups," in *2017 14th Workshop on Positioning, Navigation and Communications (WPNC)*, 2017, pp. 1–6.

[21] M. Pelka and H. Hellbrück, "S-tdoa — sequential time difference of arrival — a scalable and synchronization free approach forl positioning," in *2016 IEEE Wireless Communications and Networking Conference*, 2016, pp. 1–6.

[22] A. R. Jiménez Ruiz and F. Seco Granja, "Comparing ubisense, bespoon, and decawave uwb location systems: Indoor performance analysis," *IEEE Transactions on Instrumentation and Measurement*, vol. 66, no. 8, pp. 2106–2117, 2017.

[23] A. Alghuraid, A. Almalki, A. Alnaim *et al.*, "Development of ultra-wide-band indoor positioning system designed to control the position of a grid confined robotic platform," in *2021 4th International Symposium on Advanced Electrical and Communication Technologies (ISAECT)*, 2021, pp. 1–5.

[24] M. Wang, F. Yang, Z. Zhou, and H. Qiu, "Base station selection method for uwb indoor positioning based on tdoa fingerprint," in *2021 IEEE 5th Information Technology,Networking,Electronic and Automation Control Conference (ITNEC)*, vol. 5, 2021, pp. 1587–1593.

[25] L. Santoro, M. Nardello, D. Brunelli, and D. Fontanelli, "Scale up to infinity: the UWB Indoor Global Positioning System," in

IEEE Intl. Symposium on Robotic and Sensors Environments (ROSE). Virtual conference: IEEE, October 2021, pp. 1–8.

[26] R. M, "Review on motion capture technology," *Global Journal of Computer Science and Technology*, 2018.

[27] K. Kuru, "Planning the future of smart cities with swarms of fully autonomous unmanned aerial vehicles using a novel framework," *IEEE Access*, vol. 9, pp. 6571–6595, 2021.

[28] M. A. Limeira, L. Piardi, V. C. Kalempa *et al.*, "Wsbot: A tiny, low-cost swarm robot for experimentation on industry 4.0," in *2019 Latin American Robotics Symposium (LARS), 2019 Brazilian Symposium on Robotics (SBR) and 2019 Workshop on Robotics in Education (WRE)*, 2019, pp. 293–298.

[29] M. Rubenstein, A. Cornejo, and R. Nagpal, "Programmable self-assembly in a thousand-robot swarm," *Science*, vol. 345, no. 6198, pp. 795–799, 2014. [Online]. Available: https://www.science.org/doi/abs/10.1126/science.1254295

[30] D. Fontanelli, D. Macii, P. Wolfrumand *et al.*, "A clock state estimator for ptp time synchronization in harsh environmental conditions," in *Proc. IEEE Int. Symp. on Precision Clock Synchronization for Measurement, Control and Communication (ISPCS)*, Munich, Germany, 12-16 Sept. 2011, pp. 99–104, Best Academic Paper Award.

[31] J. Kulmer, S. Hinteregger, B. Großwindhager *et al.*, "Using decawave uwb transceivers for high-accuracy multipath-assisted indoor positioning," in *2017 IEEE International Conference on Communications Workshops (ICC Workshops)*, 2017, pp. 1239–1245.

[32] M. Frisk and A. Nilsson, "Inertial sensor and ultra-wideband sensor fusion: Precision positioning of robot platform," Ph.D. dissertation, 2014. [Online]. Available: http://urn.kb.se/resolve?urn=urn:nbn:se:uu:diva-231053

[33] I. . W. Group *et al.*, "Ieee standard for local and metropolitan area networks, part 15.4: Low-rate wireless personal area networks (lr-wpans)," *IEEE Std*, vol. 802, pp. 4–2011, 2011.

[34] DecaWave, "DW1000 Data Sheet," 2016.

[35] S. M. Kay, *Fundamentals of statistical signal processing: estimation theory*. Prentice-Hall, Inc., 1993.

[36] D. Fontanelli, F. Shamsfakhr, and L. Palopoli, "Cramer-Rao Lower Bound Attainment in Range-only Positioning using Geometry: The G-WLS," *IEEE Trans. on Instrumentation and Measurement*, vol. 70, pp. 1–14, 2021, early Access.

[37] Y. Weng, "Source localization using tdoa measurements with sensor location uncertainty," in *Proceedings of the 30th Chinese Control Conference*, 2011, pp. 5068–5072.

[38] R. Zekavat and R. M. Buehrer, *Handbook of position location: Theory, practice and advances*. John Wiley & Sons, 2011, vol. 27.

[39] A. Ledergerber and R. D'Andrea, "Ultra-wideband range measurement model with gaussian processes," in *2017 IEEE Conference on Control Technology and Applications (CCTA)*, 2017, pp. 1929–1934.

[40] C. Lian Sang, M. Adams, T. Hörmann *et al.*, "Numerical and experimental evaluation of error estimation for two-way ranging methods," *Sensors*, vol. 19, no. 3, 2019.